a reprint from Applied Optics

Effect of nonuniform spectral dome transmittance on the accuracy of infrared radiation measurements using shielded pyrradiometers and pyrgeometers

F. Miskolczi and R. Guzzi

We discuss the problem arising from the nonuniform distribution of spectral transmittance of the instrument's shielding dome. Recently, by using high-resolution atmospheric radiation software, it became possible to evaluate both the real downward IR spectral flux density and the transmitted spectral flux density of the instrument's dome. By using a simplified model we obtained a theoretical formula that describes the effect of dome transmittance on the instrument's response. By the formula, the effective dome transmittance (average dome transmittance weighted by the spectral flux density) is directly proportional to the calibration constant of the instrument. In order to obtain a quantitative relationship we computed the effective dome transmittance for several domes and model atmospheres. According to our results the maximum difference in effective dome transmittance of individual domes is 20% for Eppley-type silicon domes and 10% for polyethylene domes. These relatively large differences must be corrected when the domes are replaced. The effective dome transmittance shows strong correlation with precipitable water and the total downward IR flux density. The combined effect on the calibration factor is a maximum 2% for the Eppley domes and 5% for the polyethylene domes. By using the linear regression method these types of error can be minimized.

Introduction

There is an increasing need for high-accuracy measurements of the downward atmospheric (IR) radiation. So far the dependence of the calibration of commonly used pyrradiometers and pyrgeometers on related climatological data (air temperature, wind speed, humidity, etc.) has not been evaluated properly; therefore, the error in the measured downward IR flux density may be unacceptable.

The most commonly used nonspectral infrared radiometers are of two general types. The instrument that measures only IR radiation is called a pyrgeometer and its sensor is shielded with a material that is opaque in the visible spectral range. The second type is a pyrradiometer and it measures the total downward radiation (IR + visible). The shielding material is generally polyethylene. Pyrradiometers and pyrgeometers oeprate on the same principle. One has to monitor the equilibrium temperature of a sensor as maintained by the balance between absorbed and emitted radiative fluxes. Pyrradiometers and pyrgeometers are similar in structure, therefore they have the same fundamental sources of instrumental errors.[1,2] While the deviations of the sensor absorption characteristics from the ideal cosine law and the nonuniform absorptivity of the sensor coating in the visible and in the IR spectral range are more or less considered in the design and calibration of the instrument, not too much is known about the effect of the instrument's protective dome on the calibration and accuracy.

According to the measurements in the 3–25 μm region (400–3300 cm^{-1}), the polyethylene exhibits three major absorption peaks at 3.55, 6.9, and 14 μm. It is also known that the aging of the polyethylene dome seriously affects the transmittance characteristics by producing strong additional absorption peaks around 5 μm and considerably decreasing transmittance in the 8–12- and 2.8–3.2-μm regions (see Figs. 3 and 4).

The total amount of water vapor in a vertical air

F. Miskolczi is with the Department of Meteorology, University of Maryland, College Park, Maryland 20742. R. Guzzi is with the Istituto per lo Studio delle Metodologie Geofische Ambientali, 770 Via Emilia Est, 41100 Modena, Italy.

Received 9 December 1991.
0003-6935/93/183257-09$06.00/0.

column is highly variable, and the water vapor is known to have line-type and coninuum-type absorption characteristics over the whole IR spectrum. Theoretically, the coincidence of the strong atmosphere water vapor emission lines with the polyethylene absorption lines may introduce a water-vapor-dependent systematic error into the radiation measurements. Independent of the spectral distribution of the downward IR flux, any changes in the transmittance characteristic of the dome might be the source of calibration error.

Dome Effect

In this section we compare the responses of a shielded and an open sensor by using a simplified model.

Open sensor

It is relatively easy to obtain the relationship between the measured thermopile voltage V and the downward IR flux density F. By neglecting the temperature changes of the hot junction that are due to the Peltier effect, V will depend only on the temperature difference between the sensor and the cold junction:

$$V = c_0^S(T_A - T_S) = c_0^S \Delta T_S, \tag{1}$$

where c_0^S is the sensitivity of the thermopile, T_S is the temperature of the sensor plate, and T_A is the temperature of the cold junction. For all practical purposes the cold junction temperature is equal to ambient air temperature. Details of the computation of a thermocouple signal are discussed in Ref. 3.

If we consider only the heat exchange perpendicular to the sensor surface, the stationary energy balance equation of the sensor plate takes the next form:

$$\epsilon^S(F - \sigma T_S^4) = [c_1^S + c_2^S(w)]\Delta T_S, \tag{2}$$

where ϵ^S is the emissivity of the sensor coating, c_1^S is the conductive heat loss toward the cold junction, $c_2^S(w)$ is the heat loss that is due to convection, and w is the wind speed. The convective term might also depend on the wind direction and relative humidity. Under normal measuring conditions it is reasonable to assume that $|\Delta T_S| \ll T_A$; therefore $T_S^4 \simeq T_A^4 - 4T_A^3\Delta T_S$.

Substituting ΔT_S from Eq. (2) into Eq. (1) and taking the derivative with respect to F we get

$$R = \frac{\partial V}{\partial F} = \frac{c_0^S \epsilon^S}{c_1^S + c_2^S(w) - \epsilon^S 4\sigma T_A^3}, \tag{3}$$

where R is the response of the instrument. A typical value of R is 10 μVm^2/W. With careful design the conductive heat loss can be maintained at a small level, therefore c_1^S is generally negligible.[4] In Eq. (3) $c_2^S(w)$ is the most problematic term. Either the convective heat loss is controlled by ventilation or the wind speed and direction are monitored during the measurements. For example, in the case of the Yanishevsky net pyrradiometer the correction factor to R is 25% at 12-m/s wind speed.[5]

If the spectral emissivity of the sensor, $\epsilon_\nu^S(T)$, is constant (i.e., not dependent on the wave number and temperature),

$$\epsilon^S \equiv \frac{\int_0^\infty B_\nu(T)\epsilon_\nu^S(T)\mathrm{d}\nu}{\sigma T^4 \pi^{-1}}, \tag{4}$$

where $B_\nu(T)$ is the Planck blackbody function. In this case the calibration of the instrument does not depend on the spectral distribution of the downward IR flux by unwanted spectral selectivity. The variation of ϵ^S that is due to the degradation of the black paint coating of the sensor plate might still be significant and necessary to consider.

Shielded Sensor

To suppress the convective heat loss one can place a transparent sheet or dome over the sensor plate for shielding. In what follows we deal only with the case when the shielding is performed by a hemispherical dome. To obtain the response of a shielded sensor we must make some assumptions:

The dome has a perfectly hemispherical shape with relatively large radius compared with the size of the sensor plate.

The dome temperature is uniform on the surface of the dome.

The space between the dome and sensor is perfectly transparent in the IR.

For simplicity, processes related to the reflection are neglected.

There is no convective heat transport between the dome and the sensor.

The spectral transmittance of the dome is temperature independent.

Assume the cylindrical symmetry of the IR radiation field.

Under the above assumptions the stationary energy balance equation of the sensor plate is

$$2\pi \int_0^\infty \int_0^1 [I_\nu(\mu)\tau_\nu^D + B_\nu(T_D)\epsilon_\nu^D]\mu \mathrm{d}\mu \mathrm{d}\nu = \sigma T_S^4 + \frac{c_1^S \Delta T_S}{\epsilon^S}, \tag{5}$$

where T_D is the temperature of the dome, τ_ν^D and ϵ_ν^D are the spectral transmittance and emissivity of the dome, respectively, and $\tau_\nu^D \equiv \tau_\nu^D(T) = 1 - \epsilon_\nu^D$. $I_\nu(\mu)$ is the spectral radiance and $\mu = \cos(\theta)$, where θ is the zenith angle.

By expanding $B_\nu(T_D)$ around T_A and preserving

only the first two terms we can write

$$B_\nu(T_D) = B_\nu(T_A) - \left[\frac{\partial B_\nu(T)}{\partial T}\right]_{T=T_A} \Delta T_D, \quad (6)$$

where $\Delta T_D = T_A - T_D$. By substituting Eq. (6) into Eq. (5) and neglecting again the higher-order terms of $\Delta T_S/T_A$ and $\Delta T_D/T_A$ we get

$$F^* + \pi \int_0^\infty B_\nu(T_A)\epsilon_\nu{}^D \mathrm{d}\nu - \Delta T_D \frac{\partial}{\partial T_A} \pi \int_0^\infty B_\nu(T_A)\epsilon_\nu{}^D \mathrm{d}\nu = \sigma T_A{}^4 - \left(4\sigma T_A{}^3 - \frac{c_1{}^S}{\epsilon^S}\right)\Delta T_S, \quad (7)$$

where

$$F^* = \int_0^\infty F_\nu{}^* \mathrm{d}\nu = 2\pi \int_0^\infty \int_0^1 I_\nu(\mu)\tau_\nu{}^D \mu \mathrm{d}\mu \mathrm{d}\nu, \quad (8)$$

$F_\nu{}^*$ is the transmitted downward spectral flux density, and F^* is the total transmitted downward IR flux density. In Eq. (7) ΔT_D is obviously unknown.

It can be shown by detailed computation (see, for example, Refs. 6 and 7) that the temperature difference between the dome and the cold junction is directly proportional to the downward IR flux density. Therefore we may approximate ΔT_D as

$$\Delta T_D = c_2{}^D(w)\Delta T_S, \quad (9)$$

where $c_2{}^D(w)$ is again a constant that depends on the thermal characteristics of the dome, wind speed and wind direction, and relative humidity. The response of a shielded sensor can be obtained by using Eqs. (1), (7), and (9):

$$R^D = \frac{c_0{}^S \epsilon^S \tau_e{}^D}{c_1{}^S - \epsilon^S 4\sigma T_A{}^3[1 - \epsilon^D c_2{}^D(w)]}, \quad (10)$$

where

$$\epsilon^D = 1 - \tau^D \equiv \frac{\int_0^\infty B\nu(T_A)\epsilon_\nu{}^D \mathrm{d}\nu}{\sigma T_A{}^4 \pi^{-1}} \quad (11)$$

is the dome emissivity and

$$\tau_e{}^D = \frac{F^*}{F} = \frac{\int_0^\infty F_\nu{}^* \mathrm{d}\nu}{F} \quad (12)$$

is the definition of the effective dome transmittance. One can recognize that the responses R and R^D [Eqs. (3) and (10)] are similar. Equation (10) clearly indicates the basic effect of a shielding dome. The response of an instrument with a perfect dome ($\tau_e{}^D = 1$ and $\epsilon^D = 0$) would be completely independent of the wind, however, in general, higher dome emissivity will produce higher sensitivity to the wind. Since $\epsilon^D < 1$ and $c_2{}^D(w) \leq 1$, the most significant term that affects the linearity of the response is the effective dome transmittance. In an ideal case $\tau_e{}^D$ should not depend on the magnitude and spectral distribution of the downward IR flux density. To study the behavior of $\tau_e{}^D$ under different atmospheric conditions one has to compute the downward high-resolution spectral radiance at several zenith angles and for different model atmospheres.

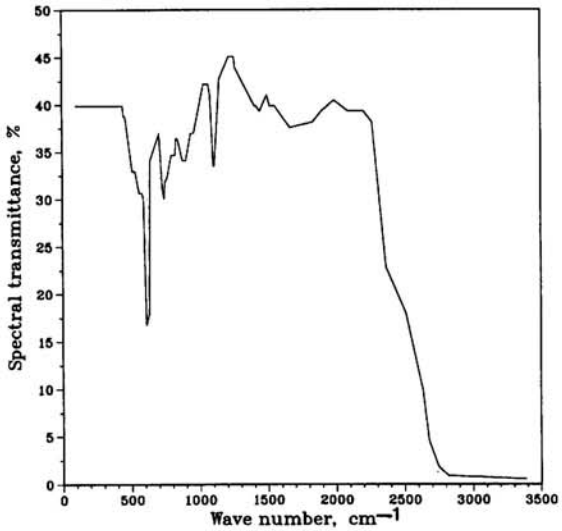

Fig. 1. Measured spectral transmittance of the D-4 dome, which is representative of the first group of Eppley silicon domes.

When we compare the measured spectral transmittance of different kinds of dome, it is sometimes useful to introduce parameters that are independent of the radiation field. These may be defined by the following equations:

$$\bar{\tau}^D = \frac{1}{\nu_2 - \nu_1} \int_{\nu_1}^{\nu_2} \tau_\nu{}^D \mathrm{d}\nu, \quad (13)$$

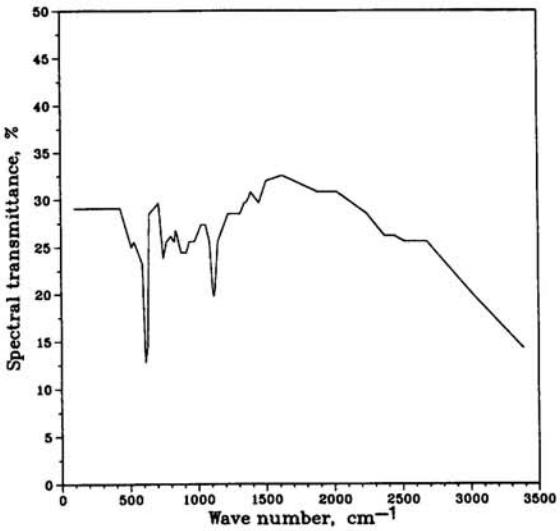

Fig. 2. Measured spectral transmittance of the D-8 dome, which is representative of the second group of Eppley silicon domes.

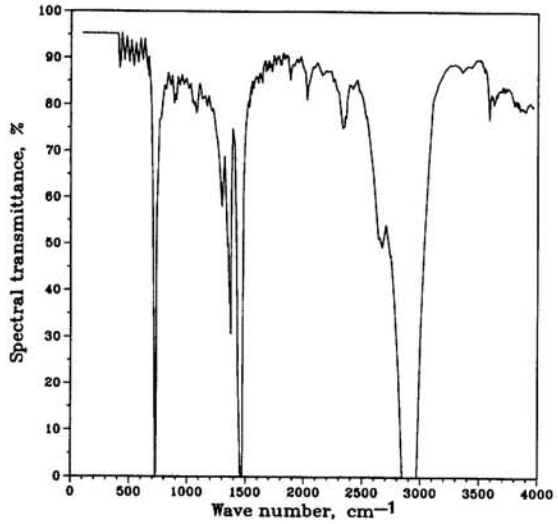

Fig. 3. Measured spectral transmittance of the D-A dome, which is the polyethylene dome.

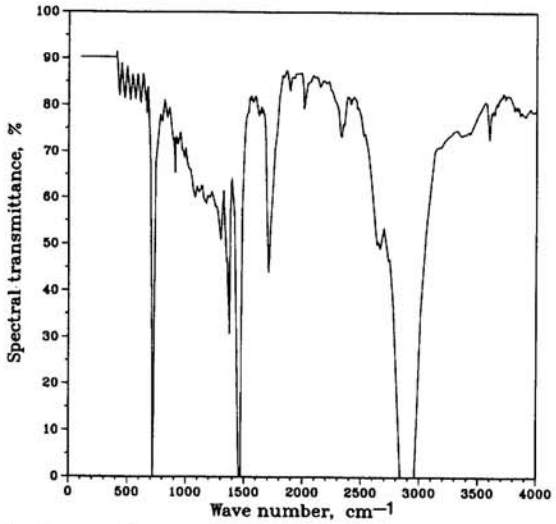

Fig. 4. Measured spectral transmittance of the D-C polyethylene dome, which is an aged polyethylene dome.

$$\kappa^D = \frac{1}{\bar{\tau}^D(\nu_2 - \nu_1)} \int_{\nu_1}^{\nu_2} |\tau_\nu{}^D - \bar{\tau}^D| \, d\nu, \qquad (14)$$

where $\bar{\tau}^D$ is the average dome transmittance and κ^D is a nonuniformity factor. A good dome is characterized by $\bar{\tau}^D \approx 1$ and $\kappa^D \approx 0$.

Computation of IR Flux Density

By definition the downward IR flux density at the surface is given by the following equation:

$$F = \int_0^\infty F_\nu d\nu = \int_0^\infty \int_0^{2\pi} \int_0^1 I_\nu(\mu, \phi)\mu d\mu d\phi d\nu$$

$$= 2\pi \int_0^\infty \int_0^1 I_\nu(\mu)\mu d\mu d\nu, \qquad (15)$$

where $I_\nu(\mu, \phi) \equiv I_\nu(\mu)$ is the monochromatic radiance at the ground and ϕ is the azimuth angle. The usual way to evaluate the wave-number integral numerically is to divide the spectral domain into several reasonably small subintervals and, by using available radiation software, to compute the averaged spectral radiance over the subinterval. The length of the subinterval depends on the required spectral resolution.

Because of the small anisotropy in the angular distribution of the downward IR radiance the integration with respect to the zenith angle can be performed by any type of simple numerical technique. In our case Eq. (15) takes the following form:

$$F = \sum_{i=1}^{N} F_{\nu_i} = \sum_{i=1}^{N} \sum_{j=1}^{M-1} \frac{I_{\Delta\nu_i}(\theta_j) + I_{\Delta\nu_i}(\theta_{j+1})}{2\pi^{-1}}$$

$$\times [\sin^2(\theta_{j+1}) - \sin^2(\theta_j)], \qquad (16)$$

where N is the number of wave-number subintervals, M is the number of zenith angles, and $I_{\Delta\nu_i}(\theta_j) = \delta\nu_i I_{\delta\nu_i}(\theta_j)$ where $I_{\delta\nu_i}(\theta_j)$ is the averaged spectral radiance over $\delta\nu_i$ in the θ_j direction and $\delta\nu_i$ is the length of a subinterval. A similar equation exists for the transmitted flux denisty:

$$F^* = \sum_{i=1}^{N} F_{\nu_i}{}^* = \sum_{i=1}^{N} \bar{\tau}_{\nu_i}{}^D F_{\nu_i}, \qquad (17)$$

where $\bar{\tau}_{\nu_i}{}^D$ is the dome transmittance averaged over $\delta\nu_i$.

Table 1. Precipitable Water (u in g/cm²), Surface Air Temperature (T_A in K), and the Downward Flux Density (F in W/m²) of the Different Atmospheres[a]

Profile	Remarks	u	T_A	F	ΔF
P-S1	Denver, 31 October 1988, 14:00 GMT	0.637	277.8	241.3	−93.82
P-S2	Denver, 31 October 1988, 20:00 GMT	0.403	294.4	269.8	−153.4
P-S3	Denver, 1 November 1988, 11:00 GMT	0.377	278.0	233.2	−102.9
P-TR	Tropical	4.170	299.7	396.5	−58.07
P-MS	Mid-latitude summer	2.960	294.2	351.6	−70.40
P-MW	Mid-latitude winter	0.860	272.2	223.2	−85.60
P-AS	Subarctic summer	2.100	287.2	301.9	−82.67
P-AW	Subarctic winter	0.420	257.2	172.3	−71.70
P-US	Standard, USST-1976	1.430	288.2	287.7	−100.8

[a]In the last column $\Delta F = F - \sigma T_A{}^4$ and $\sigma = 5.67032 \times 10^{-8}$ W/(m² K⁴). The product of ΔF with the instrument response is equal to the measured signal. GMT, Greenwich mean time; USST, U.S. Standard Atmosphere.

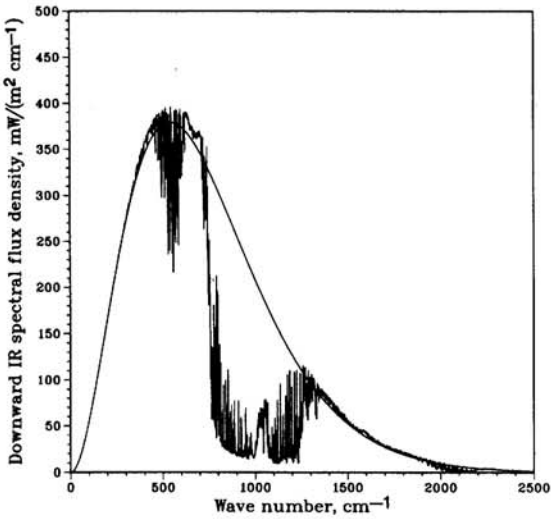

Fig. 5. Downward IR spectral flux density versus wave number computed for profile P-S1 at Denver on 31 October 1988 at 14:00 GMT. Spectral resolution is 1 cm^{-1}, u = 0.637 g/cm^2, T_A = 277.8 K.

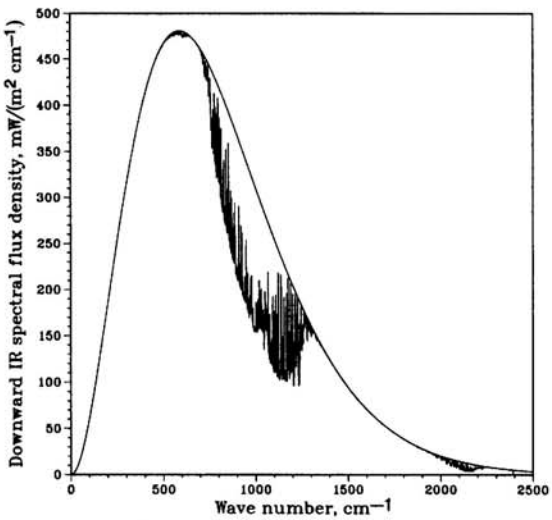

Fig. 7. Downward IR spectral flux density versus wave number computed for profile P-TR (tropical model atmosphere). Spectral resolution is 1 cm^{-1}, u = 4.17 g/cm^2, T_A = 299.7 K.

In this study we deal only with the 110–3390-cm^{-1} spectral region. The reason for this wave-number limitation is purely practical, i.e., most of the polyethylene transmittance measurements are made inside this interval. Besides, more than 90% of the thermal IR flux density is within this spectral range. In the 110–3390-cm^{-1} interval, $I_{\delta\nu_i}(\theta_j)$ was computed with 1-cm^{-1} resolution ($\delta\nu_i \equiv 1\ cm^{-1}$, N = 3281) and for six zenith angles (0°, 30°, 45°, 60°, 80°, and 90°).

Although the LOWTRAN and fast atmospheric signature code (FASCODE) computer codes were also available, for the sake of higher accuracy, the computation of $I_{\delta\nu_i}(\theta_j)$ was performed by using the high-resolution atmospheric radiance/transmittance code (HARTCODE) radiation software.[8] Compared with other codes and with high-resolution spectral radiance measurements the accuracy of the HARTCODE is quite sufficient for our relatively low resolution modeling purpose.

Input Data

For this study eleven high-resolution measured transmittance spectra of two types of dome were available. From the National Atmospheric Radiation Centre in Downsview, Canada, we obtained the plotted transmittance spectra of eight Eppley (silicon) IR domes.[9] The measurements were taken in the 400–3333-cm^{-1} interval. The temperatures during the measurements were not recorded. Figures 1 and 2 show two measured Eppley IR dome transmittance spectra.

Another three measured transmittance spectra of polyethylene domes were obtained from the Department of Radiation of the Institute for Atmospherics Physics in Budapest, Hungary.[10] In this case the

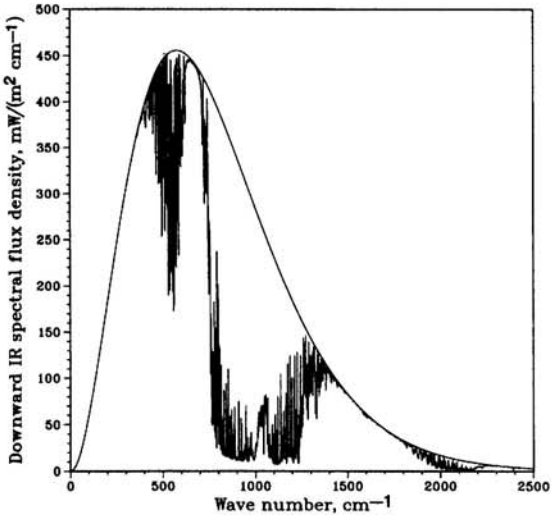

Fig. 6. Downward IR spectral flux density versus wave number computed for profile P-S2 at Denver on 31 October 1988 at 20:00 GMT. Spectral resolution is 1 cm^{-1}, u = 0.403 g/cm^2, T_A = 294.4 K.

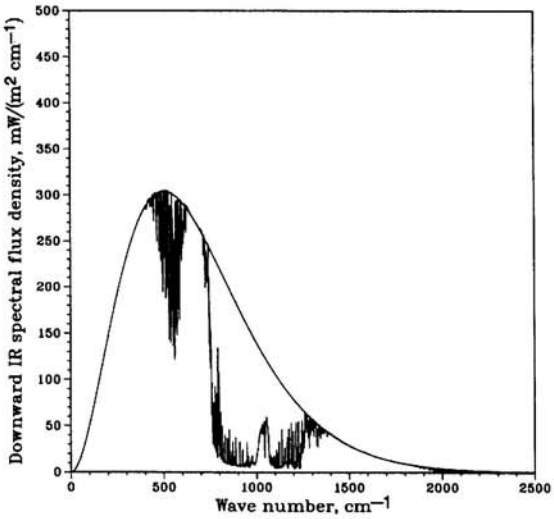

Fig. 8. Downward IR spectral flux density versus wave number computed for profile P-AW (subarctic winter model atmosphere). Spectral resolution is 1 cm^{-1}, u = 0.420 g/cm^2, T_A = 257.2 K.

measurements were taken at room temperature and in the 400–4000-cm^{-1} spectral interval with 2-cm^{-1} resolution. Two polyethylene domes were new and one had been in use for approximately a year. The transmittance spectra of a new and old polyethylene dome are plotted in Figs. 3 and 4.

Unfortunately, no details of the IR spectral reflectance of the domes were given. It is known, however, that assuming normal incidence the spectral reflectance of the polyethylene is approximately 1–3% and there are small local maxima at the wave numbers at which the spectral transmittance is low. Similarly, we had no information on the temperature dependence of the spectral transmittance, but in the temperature range at which the domes operate, the transmittance is fairly constant.[10]

The computations of the downward flux density spectra were based on three measured atmospheric temperature and water vapor profiles and six model profiles. The radiosonde measurements were supplied with simultaneous high-resolution downward spectral radiance measurements in the 0.0° zenith angle. The spectral measurements were taken in the 600–1400-cm^{-1} spectral range with 0.5-cm^{-1} resolution by the high-resolution interferometer sounder instrument.[11] These high-quality spectral measurements were used to test the accuracy of the HARTCODE computations. The other six profiles were the five standard LOWTRAN model atmospheres and the U.S. Standard Atmosphere 1976. The details of the input profiles are summarized in Table 1, and some computed downward IR flux density spectra for four selected profiles are presented in Figs. 5–8.

In Fig. 9 we compare the computed flux density spectra of the tropical model atmosphere that contains 4.17-g/cm^2 precipitable water with the same atmosphere that contains no water at all. The dependence of the flux density on the water content is shown in Fig. 10. These two figures clearly indicate the importance of the atmospheric water vapor in the IR radiative transfer of the Earth's atmosphere. In Fig. 11 we plotted the dependence of the downward radiation on the zenith angle for three model atmospheres.

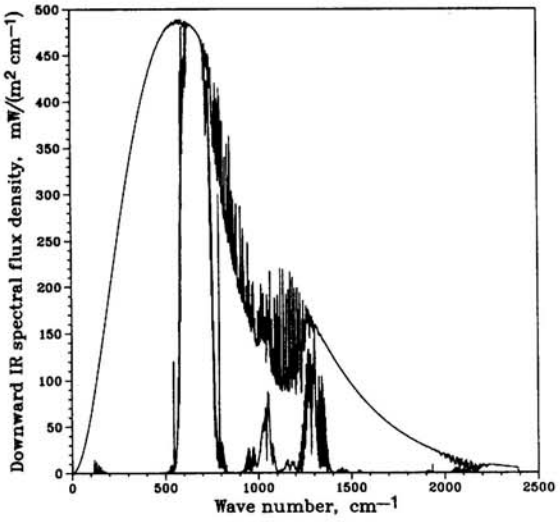

Fig. 9. Effect of the atmospheric water vapor on the downward spectral flux density. The upper curve was computed for the tropical model atmosphere, taking into consideration all seven major absorbers (H_2O, CO_2, O_3, N_2O, CO, CH_4, and O_2). In this case $F = 396.5\ W/m^2$. The lower curve was obtained by the same computation but without H_2O. The total flux density reduced to $F = 96.62\ W/m^2$.

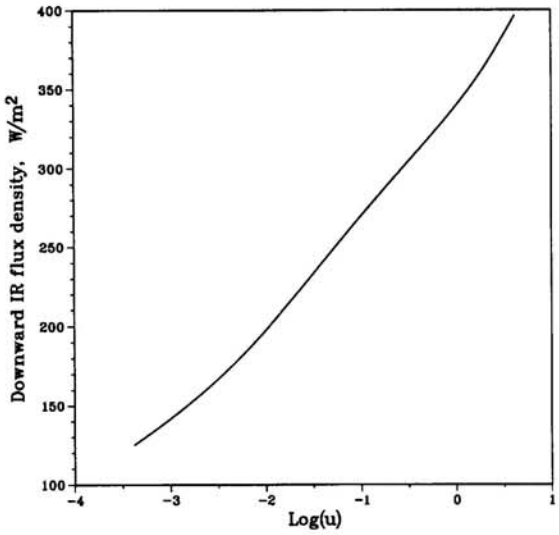

Fig. 10. Dependence of the total downward IR flux density on the water vapor content of the atmosphere. Log(u) is the ten based logarithms of precipitable water (u is in g/cm^2). In this numerical experiment the water vapor content of the tropical model atmosphere was gradually decreased from 4.17 g/cm^2 to zero. The shape of the water vapor profile was not changed.

Results

Independent of the spectral structure of the real downward IR flux density we can compare the aver-

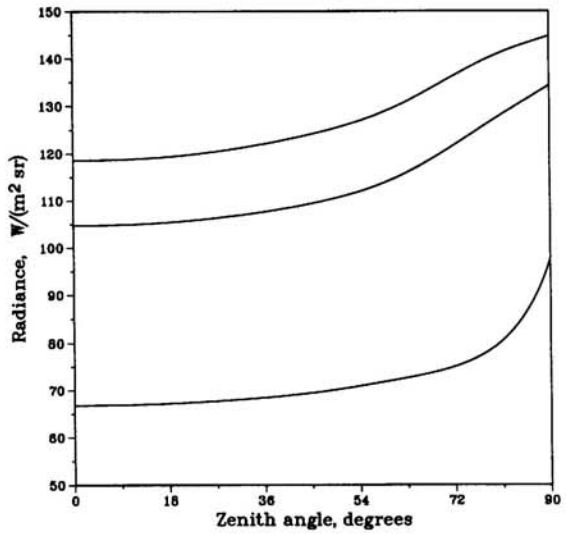

Fig. 11. Angular anisotropy in the downward radiance. The uppermost curve belongs to the tropical atmosphere, the lowermost curve was computed for the mid-latitude winter profile, and the curve in between belongs to the mid-latitude summer profile. This anisotropy might disturb the uniform temperature distribution on the surface of the dome.

Table 2. Average Measured Dome Transmittance $\bar{\tau}^D$, Nonuniformity Factors κ^D, and the Dome Transmittance τ^D at Two Different Temperatures (250 and 290 K)[a]

Dome	Remarks	$\bar{\tau}^D$	κ^D	$\tau_{250}{}^D$	$\tau_{290}{}^D$	$\Delta\tau^D$
D-1	Eppley (silicon)	29.82	9.19	33.19	33.53	.34
D-2	Eppley (silicon)	35.16	3.48	34.86	35.09	.23
D-3	Eppley (silicon)	26.05	9.41	30.14	30.37	.23
D-4	Eppley (silicon)	27.85	14.1	36.33	36.52	.19
D-5	Eppley (silicon)	35.65	2.54	34.48	34.53	.05
D-6	Eppley (silicon)	35.11	4.19	35.62	35.74	.12
D-7	Eppley (silicon)	34.43	3.51	34.06	34.21	.15
D-8	Eppley (silicon)	26.29	3.58	26.73	26.78	.05
D-A	Polyethylene (new)	74.79	17.7	84.81	82.91	−1.9
D-B	Polyethylene (new)	73.15	17.6	82.80	81.03	−1.8
D-C	Polyethylene (old)	67.72	17.0	77.56	75.08	−1.7

[a]In the last column $\Delta\tau^D = \tau_{290}{}^D - \tau_{250}{}^D$. The values are given in percent and the wave-number interval is from 110.0 to 3390.0 cm^{-1}.

Table 3. Computed Effective Transmittance of the Eppley Domes in Percent

Profile	D-1	D-2	D-3	D-4	D-5	D-6	D-7	D-8
P-S1	33.30	34.84	30.28	36.27	34.61	35.95	34.90	27.27
P-S2	33.48	35.02	30.44	36.40	34.73	36.13	35.12	27.46
P-S3	33.31	34.89	30.29	36.32	34.66	36.02	34.97	27.35
P-TR	33.54	35.06	30.41	36.41	34.55	35.82	34.56	26.99
P-MS	33.46	34.98	30.35	36.34	34.54	35.82	34.63	27.04
P-MW	33.23	34.79	30.22	36.25	34.59	35.90	34.78	27.21
P-AS	33.36	34.89	30.29	36.27	34.53	35.83	34.70	27.10
P-AW	33.15	34.79	30.19	36.32	34.68	35.98	34.77	27.27
P-US	33.37	34.88	30.32	36.27	34.56	35.89	34.83	27.20

age dome transmittance [$\bar{\tau}^D$ in Eq. (13)], the nonuniformity factors [κ^D in Eq. (14)], and the dome transmittance at different temperatures [τ^D in Eq. (11)]. The results of these calculations are summarized in Table 2. With regard to the data in Table 2 we might immediately conclude that none of the Eppley domes is interchangeable. The maximum difference between the transmittance of the individual domes is more than 20%.

In addition, if we consider the dependence of τ^D on the temperature as an indication of the variation of the $\bar{\tau}^D$ with the wave number (on a smaller scale) we can distinguish two groups of Eppley dome. (Note that τ^D is a weighted average with respect to the Planck function.) In the first group (D-1, D-2, D-3, and D-4), $\bar{\tau}^D$ is generally larger than τ^D while κ^D and $\Delta\tau^D$ are relatively large positive numbers. In the second group (D-5, D-6, D-7 and D-8), τ^D is close to $\bar{\tau}^D$ and κ^D and $\Delta\tau^D$ are small values.

The basic differences between the two kinds of dome are the significantly smaller transmittance of the Eppley IR domes, the larger values of the nonuniformity factors, and the relatively large negative values of $\Delta\tau^D$ of the polyethylene domes. It is also evident that the aging of the polyethylene dome is related to the lower value of the average transmittance. Since the maximum difference between the individual dome transmittance is more than 10%, these domes are also not interchangeable. The variation of τ^D with temperature implies that there must be a correlation between F and $\tau_e{}^D$.

The effective dome transmittance was computed for each profile and each dome. The results are included in Tables 3 and 4. The usual statistical parameters of the linear regression analysis are included in Table 5. From the results we can conclude that the variations of $\tau_e{}^D$ with respect to the different atmospheric profiles are small compared with the ones for different domes. The dependence of $\tau_e{}^D$ on the water vapor is related to the dependence of the downward spectral radiance on the continuum- and line-type absorption of water vapor. Because of the continuum-type absorption, if we increase the water vapor content, the spectral radiance will increase similar to the Planck function, i.e., the maximum will be shifted toward the larger wave numbers, and $\tau_e{}^D$ will follow the behavior of τ^D. (Assume a negative vertical temperature gradient.) Because of the line-

Table 4. Computed Effective Transmittance of the Polyethylene Domes (in percent)

Profile	D-A	D-B	D-C
P-S1	83.85	81.72	77.71
P-S2	83.27	81.14	77.14
P-S3	83.58	81.43	77.55
P-TR	82.62	80.70	75.45
P-MS	82.91	80.95	76.01
P-MW	84.36	82.22	78.19
P-AS	83.37	81.35	76.77
P-AW	85.15	82.94	79.20
P-US	83.43	81.37	77.03

Table 5. Average Effective Dome Transmittance $\bar{\tau}_e^D$, Standard Deviations σ_e, Maximum Difference $\Delta\tau_e^D$, and the Regression Coefficients Related to the Water Amount and the Total Downward IR Flux Density (r_u and r_F, respectively)

Dome	$\bar{\tau}_e^D$	σ_e	$\Delta\tau_e^D$	r_u	r_F
D-1	33.36	0.1256	0.3925	0.6860	0.9013
D-2	34.90	0.0968	0.2687	0.6303	0.8240
D-3	30.31	0.0797	0.2441	0.4797	0.7506
D-4	36.32	0.0596	0.1663	0.3885	0.4807
D-5	34.60	0.0693	0.1956	−0.7489	−0.6326
D-6	35.93	0.1038	0.3107	−0.7870	−0.5862
D-7	34.81	0.1734	0.5598	−0.8253	−0.5539
D-8	27.21	0.1472	0.4604	−0.9020	−0.7102
D-A	83.62	0.7644	2.5311	−0.6990	−0.9171
D-B	81.54	0.6844	2.2400	−0.6475	−0.8873
D-C	77.23	1.1229	3.7556	−0.8487	−0.9845

type absorption the increased amount of water vapor will increase the spectral radiance selectivity. If the dome absorbs at the wave numbers of the water vapor absorption lines the increased spectral radiance will not contribute to F^*; therefore τ_e^D will always decrease. The overall effect of water vapor on τ_e^D is governed by the basic tendency of the dome transmittance (indicated by $\Delta\tau^D$) and the result of the two competing processes related to the continuum- and line-type absorption.

In the first group of Eppley domes and the polyethylene domes the behavior of τ^D and τ_e^D is similar, the correlation coefficient r_u is small, while r_F is large. This means that the effect of line-type H_2O absorption is suppressed by the larger effect of F and the continuum absorption.

In the second group of domes the small positive $\Delta\tau^D$ and the large negative correlation coefficients r_u clearly indicate the effect of line-type water vapor absorption on τ_e^D. The small r_F is also not surprising. As an example, Fig. 12 shows how the τ_e^D of the D-8 (Eppley) dome depends on the precipitable water content of the atmosphere. In practice the quantitative correction of the instrument calibration with respect to the dependence of u and F can be performed by using the following equation:

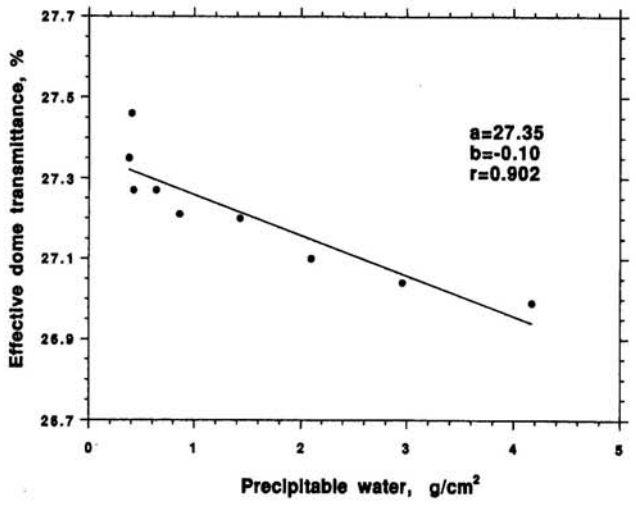

Fig. 12. Dependence of the effective dome transmittance, τ_e^D, on the precipitable water content of the atmosphere u for the D-8 (Eppley) dome.

Table 6. Regression Coefficients A_0, A_1, and A_2 and the Correlation Coefficients r_{uF} Related to Eq. (18)

Dome	A_0	A_1	A_2	r_{uF}
D-1	32.60	−0.08733	0.003202	0.9729
D-2	34.38	−0.05789	0.002206	0.8849
D-3	29.78	−0.08416	0.002388	0.9192
D-4	36.15	−0.01560	0.000689	0.5006
D-5	34.59	−0.05428	0.000329	0.7516
D-6	35.75	−0.12240	0.001299	0.8553
D-7	34.27	−0.26450	0.000364	0.9773
D-8	27.01	−0.18100	0.001712	0.9539
D-A	88.27	0.53220	−0.01979	0.9882
D-B	85.90	0.55820	−0.01888	0.9852
D-C	82.72	0.30790	−0.02162	0.9952

$$\tau_e^c(u, F) = A_0 + A_1 u + A_2 F, \qquad (18)$$

where $\tau_e^c(u, F)$ is the actual computed effective dome transmittance and u and F are now measured quantities (u is in g/cm^2 and F is in W/m^2). A_0, A_1, and A_2 are regression coefficients and were determined by a simple least-squares linear regression. The numerical values for each dome are presented in Table 6.

The computation of $\tau_e^c(u, F)$ for other domes requires the measured spectral dome transmittance, which can be obtained from the manufacturer, and the computed high-resolution flux density spectra of the nine model atmospheres, which are available from the authors upon request.

Conclusions

In the case of Eppley domes the effect of water vapor on the calibration is very small, always less than 2.0%. Because of the low effective dome transmissivity the calibration of the Eppley instrument is more sensitive to the wind. The water vapor effect on the calibration is a maximum of 5.0% for polyethylene domes. Because of the large differences between the individual dome transmittances (more than 20% for Eppley domes and 2.5% of the new polyethylene domes) recalibration of the instrument is necessary when the dome is replaced. The aging of the polyethylene dome will change the calibration of the instrument by approximately 10% within a year; therefore, frequent recalibration of the pyrradiometer is advisable.

The authors express their thanks for the financial support received from the International Centre for Theoretical Physics, Trieste, Italy. The assistance of B. McArthur with the National Atmospheric Radiation Centre, Downsview, Canada, and Z. Nagy, A. Revesz, and Z. Toth with the Department of Radiation, Institute for Atmospheric Physics, Budapest, Hungary, in obtaining the high-resolution IR transmittance spectra of the different kinds of dome is also greatly acknowledged.

References

1. B. Albrecht and S. K. Cox, "Procedures for improving pyrgeometer performance," J. Appl. Meteorol. **16,** 188–197 (1976).
2. A. Weiss, "On the performance of pyrgeometers with silicon domes," J. Appl. Meteorol. **20,** 962–965 (1981).
3. W. L. Wolfe and G. J. Zissis, *The Infrared Handbook* (Environmental Research Institute of Michigan, Ann Arbor, Mich., 1985).
4. L. Aldos-Arboledas, J. Vida, and J. L. Jimenez, "Effects of solar radiation on the performance of pyrgeometers with silicon domes." J. Atmos. Ocean Technol. **5,** 666–670 (1988).
5. J. Oliveri, "Measurement of Longwave Downward Irradiance using a 'PIR' pyrgeometer," in *Radiation and Climate,* WMO/TD No. 453 (World Meteorological Organization, Geneva, 1991), App. B.
6. M. R. Martin and R. D. Anson, *An Introduction to Meteorological Measurements and Data Handling for Solar Energy Applications,* DOE/ER-0084 (U.S. Department of Energy, Washington, D.C., 1980), pp. 6.1–6.14.
7. K. L. Coulson, *Solar and Terrestrial Radiation: Methods and Measurements* (Academic, New York, 1975).
8. F. Miskolczi, R. Guzzi, R. Rizzi, and M. Bonzagni, *IRS '88: Current Problems in Atmospheric Radiation* (Deepak, Hampton, Va., 1989), pp. 388–391.
9. B. McArthur, National Atmospheric Radiation Centre, Downsview, Canada (personal communication, 1991).
10. L. Nagy, A. Revesz, and Z. Toth, Department of Radiation, Institute for Atmospheric Physics, Budapest, Hungary (personal communication, 1991).
11. R. O. Knuteson, Space Science and Engineering Center, University of Wisconsin, Madison, Wis. (personal communication, 1991).